Acoustic Filters for RF Communication: Applications, Recent Advances & Challenges

You Qian, Ying Zhang, Shashwat Bhattacharya, Wenjia Yang, Chen Liu, Yao Zhu
Institute of Microelectronics, Agency for Science, Technology and Research (A*STAR), Singapore
Email: zhuya@ime.a-star.edu.sg

INTRODUCTION

Let's imagine you're at a concert. The music is blasting, and everyone's having a good time. Now, you only want to hear the melodious voice of the lead singer, but you're getting drowned in the thumping bass and the crashing cymbals. This is akin to the problem that mobile communication faces. The solution? Filters. We're talking about two nifty tools in the Microelectromechanical Systems (MEMS) toolkit: Surface Acoustic Wave (SAW) and Bulk Acoustic Wave (BAW) filters, which are like advanced audio engineers at the soundboard, carefully tuning and adjusting the signals to give you the best performance.

The preference for acoustic wave technology in certain applications stems primarily from the distinct properties of wave propagation. When it comes to wave travel, electromagnetic (EM) waves are indeed the fastest, registering speeds of 3×10^8 m/s in air. By contrast, acoustic waves in solid materials operate at a more leisurely pace, with speeds ranging from 4,000 m/s to 12,000 m/s. The notable velocity gap between acoustic and electromagnetic waves results in a remarkable decrease in the physical size required to confine a wave. Specifically, the dimensions of SAW or BAW filters are around 10,000 times smaller than those required for electromagnetic wave confinement. For the current fourth-generation (4G) and coming fifth-generation (5G) radio frequency (RF) communication standard, an electromagnetic wave's wavelength measure about 0.1-10 m, while the acoustic wavelength in a solid material is just a few µm. This pronounced difference highlights the inherent advantages of acoustic wave technology in engineering miniaturized filtering systems in the 1-10 GHz range for RF communications.

Both BAW and SAW resonators harness the power of piezoelectric materials to facilitate conversion between electrical energy and acoustic energy, leading to resonance within their uniquely structured devices. Piezoelectric materials are integral to this process because of their unique ability to convert electrical energy into mechanical vibrations and vice versa. When an electrical field is applied to these materials, it induces a mechanical strain, generating an acoustic wave. Similarly, applied mechanical stress or vibration can produce a change of electrical charge.

In a BAW resonator, the piezoelectric material is sandwiched between two electrodes, forming a parallel plate capacitor structure (Figure 1). When an alternating electrical signal is applied to the electrodes, it produces a mechanical vibration in the thickness direction of piezoelectric material, generating an acoustic wave. This wave reflects back and forth between the two electrodes, creating a standing wave distributed in the bulk of the stack and causing the device to resonate at a specific frequency mainly determined by the thickness and the acoustic phase velocity [1]. To prevent the acoustic from propagating into the substrate, an air cavity or a Bragg mirror is constructed under the device. Usually, the BAW resonators with air-cavity underneath are named film bulk acoustic resonators (FBAR), and the ones with Bragg mirror underneath are named solid mounted resonators (SMR).

SAW resonators (Figure 1) operate on a similar principle, but the acoustic waves are actuated and propagate along the surface of the piezoelectric material. The electrical signal is applied to an interdigitated transducer (IDT), composed of two interlocking sets of metallic fingers deposited on the surface of the piezoelectric substrate. The alternating electric fields from the IDT induce a mechanical strain in the substrate, generating a surface acoustic wave. Thus, the resonant frequency is mainly determined by the pitch dimension of the IDT. This wave travels laterally along the surface of the substrate and confines the wave within the desired region, grating reflectors placed on either side of the IDT are designed to reflect the surface waves.

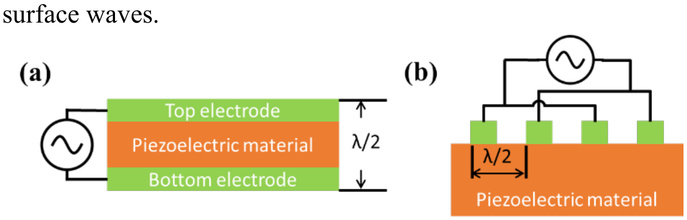

Figure 1 (a) BAW resonator structure,(b) SAW resonator structure

In both BAW and SAW resonators, the resonant frequencies are largely determined by the geometry design of the device structure and the properties of the piezoelectric material used. Through careful design and material selection, these devices can be tuned to resonate at specific frequencies, making them invaluable in a wide range of filtering and signal-processing applications.

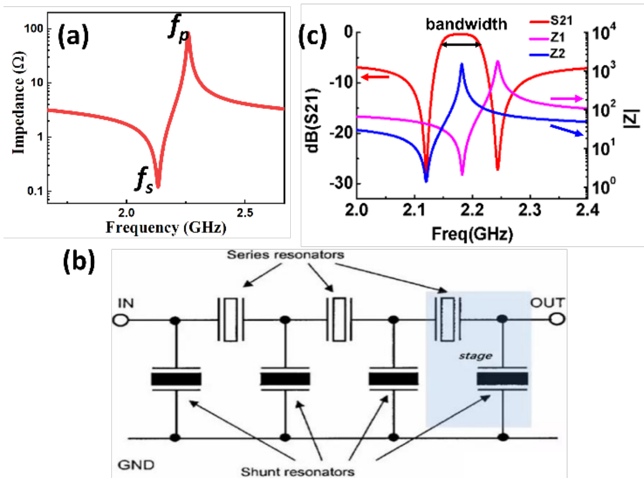

Figure 2 (a) A typical frequency spectrum of the impedance of SAW/BAW resonator; (b) topology of a typical ladder filter; (c) insertion loss of the ladder filter and the relationship with series and shunt resonator.

A typical frequency spectrum of the impedance of a SAW/BAW resonator is shown in Figure 2 (a). The resonator has the lowest impedance at the series frequency (f_s) and the highest impedance at the parallel frequency (f_p). Both BAW and SAW filters commonly employ the ladder-type filter topology (Figure 2 (b)), comprising series and shunt resonators arranged like a ladder. Series resonators are located directly along the signal path. They function like gates that let certain frequencies through while blocking others. All series resonators have a similar resonant frequency – the frequency at which it allows signals to pass with the least resistance. Shunt resonators, on the other hand, are connected parallelly between the signal path and the ground. You can imagine them as side roads diverting traffic away from the main road. When a signal of a particular frequency travels down the signal path, it can be diverted into a shunt resonator, thus be removed from the signal path. Similar to series resonators, all shunt resonators have another resonant frequency, normally lower than the series resonators' one [2].

"In commercial products, BAW filters excel in high-frequency (>2.5 GHz) applications with improved performance characteristics, while SAW filters are cost-effective and well-suited for low-frequency (<2.5 GHz) applications. The selection between BAW and SAW is contingent on the specific application needs, considering factors like operating frequency, performance requirements, production cost, and power handling capabilities. In this review, the authors will not retrospect much on the glorious history and the extraordinary success of the SAW/BAW in the RF filtering market for the last several decades, but will focus on cutting-edge development in recent years for the next-generation requirements and applications.

PERFORMANCE IMPROVEMENT APPROACHES FOR CURRENT SAW/BAW RESONATORS & FILTERS

The pursuit of enhanced performance in RF resonators and filters is a continuous endeavor, with substantial advancements being made in recent years. Researchers are relentlessly striving to increase the quality factor (Q) and effective coupling coefficient (k^2_{eff}) of the SAW and BAW resonators, for a larger bandwidth and a steeper roll-off of the filters. As a testament to this, a high-performance variant of SAW, known as Incredibly-High-Performance Surface Acoustic Wave (IHP-SAW), has been developed. Additionally, advancements in BAW have led to the introduction of Scandium-doped Aluminum Nitride (ScAlN) as a novel material choice. Further design innovations, including lithographically tunable BAW, have also been explored, adding to the repertoire of strategies aimed at optimizing RF resonator and filter performance.

A. IHP SAW devices

Continuous improvements in SAW devices and many modifications symbolize a significant enhancement in the ability to handle high-frequency signals. A key breakthrough was the creation of the IHP-SAW in 2016 [3], a revolutionary variant of SAW technology.

Historically, SAW devices primarily used 42 degrees YX cut lithium tantalate (42YX-LT) as the substrate, chosen for its ability to limit acoustic wave radiation losses. However, it's important to note that with 42YX-LT, eliminating these losses remains unachievable, with remaining losses mainly due to shear wave motions. IHP-SAW technology introduces a new approach, using a thin Lithium Tantalate (LT) plate designed to propagate leaky SAW on a Silicon (Si) substrate. This advancement employs a thin layer of a piezoelectric material—either lithium tantalate (LT) or lithium niobate (LN)—bound to a support substrate. The thickness of this piezoelectric layer is generally less than the SAW wavelength, typically in the submicron scale [4].

Unlike traditional 42YX-LT SAW, which suffers acoustic leakage loss from bulk acoustic wave radiation, the innovative IHP SAW approach encapsulates the bulk acoustic wave within a sub-wavelength thickness LT layer, consequently improving quality factor (Q). The faster shear waves are reflected at the interface between the substrate with high velocity and the low velocity layer and are then directed into the LT layer, mimicking the behavior of optical waveguides (Figure 3).

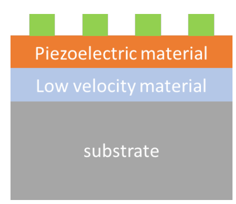

Figure 3 IHP SAW resonator structure

The IHP SAW methodology was first proposed by Murata, this development was made possible thanks to advancements in fabrication methods, which offered precise control over thin film cut from bulk piezoelectric materials. The new approach has yielded impressive results, with a Bode-Q value surpassing 6000 at 0.9 GHz to over 1900 at 3.5 GHz [5], triple the performance of conventional 42YX-LT SAW resonators. It also boasts a minimal (temperature coefficient of frequency) TCF of -8 ppm/°C. The incorporation of a SiO_2 layer beneath the piezoelectric layer aligns the thermal expansion more closely with the substrate, providing a counterbalancing TCF against the LN layer. This feature enhances the device's thermal stability, making it significantly less sensitive to temperature fluctuations.

B. Sc doped AlN film for higher coupling coefficient

The resonator holds significant importance in the design of an acoustic wave filter, with its k^2_{eff} being a key element in determining the filter's bandwidth. The electro-mechanical coupling coefficient (k_t^2) of the piezoelectric material is a prominent factor affecting the k^2_{eff} of the device.

Back in 2009, it was discovered that doping Scandium (Sc) into AlN, which is the traditional piezoelectric material for BAW resonators, can effectively enhance the intrinsic piezoelectric coefficient, subsequently leading to an increase in the resonator's $k^2_{eff,}$ from a range of 6-7% to upwards of 15%. [6]. Figure 4 depicts the crystal structure of $Sc_xAl_{1-x}N$, where x signifies the Sc doping level. The introduction of Sc dopants results in lattice distortion, which triggers a structural phase transition. This transition consequently boosts the film's responsiveness to pressure in the c-axis direction. Theoretically, higher Sc concentration in the ScAlN leads to higher k_t^2 of the piezoelectric film. It should be noted that a realistic resonator design also requires acknowledging other elements, such as the film quality, stack thickness, electrode material and topology, and so on. Figure 4 (b) shows the k^2_{eff} of the FBAR, which we measured. The FBAR has the same stack and lateral dimension but we fabricated with different Sc concentrations. The results indicate the efficiency of using ScAlN for BAW resonators' k^2_{eff} improvement.

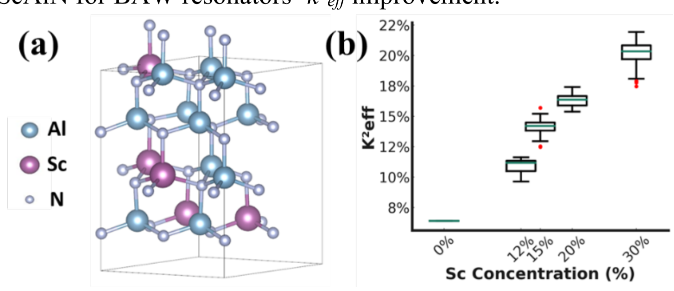

Figure 4. (a) Crystal structure of ScAlN [6] (b) The effective coupling coefficient of FBAR resonators based on ScAlN with different Sc concentrations.

Besides traditional BAW resonators like FBAR and SMR, ScAlN films are also widely utilized in other resonator structures utilizing plate modes. In [7], a Lame mode resonator composed of 20% Sc-doped AlN demonstrates a k^2_{eff} of 7.83%, operating at 2.563 GHz. More recently, Z. Luo et al. [8] has presented work [8] featuring a laterally vibrating mode resonator (LVR) that utilizes 30% Sc-doped AlN, achieving a k^2_{eff} of 9.7% and a loaded quality factor of 1141.5, operating around 305 MHz.

Although high k^2_{eff} is achieved, doping Sc also introduces challenges to film deposition and drawbacks to the devices. Films with higher Sc% deposited by physical vapor deposition (PVD) tend to have more abnormally oriented grains, more compressive in-plane stress, and higher dielectric loss, which needs more effort to optimize the film quality and uniformity. The elasticity of the ScAlN decreases with the increase of Sc%, along with the larger density, leading to the lower resonant frequency with the same stack thickness. The quality factor of devices will also drop with the increase of Sc%. Finding a balance between the k^2_{eff} and other performances is critical for the wide-range commercialization of this promising piezoelectric material.

C. lithographically frequency- adjustable BAW

Unlike SAW filters, BAW filters can only support a single band per chip due to the thickness-determined frequency. Given that filters for over 70 frequency bands are needed in the current RF communication framework, and this number is continuously increasing with more bands allocated, dedicating individual chips for each band is less and less cost-efficient nor feasible due to the expense and area overhead.

To overcome the frequency limitation of BAW resonators, various novel resonator structures with thin piezoelectric film and IDT electrodes have been proposed, in which the resonant frequency is not only determined by the thickness but also the pitch of electrode fingers. Figure 5 (a) shows a traditional Lamb wave resonator structure with only IDT on top surface of piezoelectric layer and no bottom electrode. Although the frequency is lithographically adjustable, the k^2_{eff} is generally much lower than that of BAW resonators, necessitating initiatives to boost it.

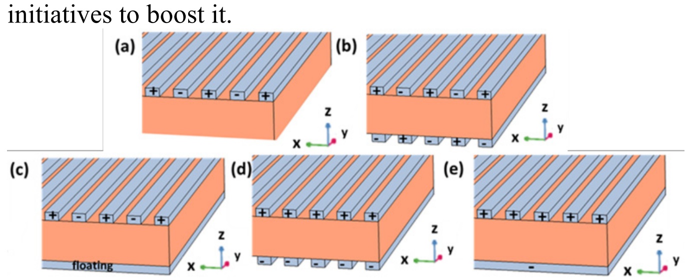

Figure 5 (a) Conventional Lamb wave resonators (b) LCAT mode resonator (c) modified LCAT mode resonator (d) 2DMR or CBAR mode resonator (e) modified BAW-like resonator

For this purpose, one approach is to couple the lateral Lamb wave mode with the thickness extensional mode, taking advantage of the high longitudinal piezoelectric coefficient in the AlN and ScAlN materials. Figure 5 (b) shows a double-sided interdigital transducer (IDT) with alternating electrical polarity, with the opposite side of each electrode possessing a different polarity. This arrangement is referred to as a Laterally Coupled Alternating Thickness (LCAT) resonator [9] or Cross-Sectional-Lamé-Mode Resonator (CLMR) [10]. In this structure, the thickness mode is triggered between each pair of top and bottom electrodes, with a phase offset of 180° between one electrode finger pair and its neighbors. At the same time, the lateral mode is excited by the lateral electric field across adjacent interdigitated fingers. As the operating frequency increases, technical challenges arise from the need to pattern fine bottom electrodes and deposit high-quality AlN films on such finely patterned electrodes. To overcome this, a modified LCAT [11] has been developed, as shown in Figure 5 (c), where a floating bottom electrode plate replaces the patterned IDT bottom electrode. However, this adjustment leads to a lower coupling coefficient due to the weakened electric field between the top and bottom electrode. Figure 5 (d) illustrates another type of electrode arrangement, which also includes double-patterned electrodes. However, here, the top and bottom electrodes are electrically connected to "+" and "-" respectively. This configuration, known as a Two-Dimensional-Mode Resonator (2DMR) [12] or Coupled Bulk Acoustic Resonator (CBAR) [13], can be seen as multiple individual "FBAR" cells acoustically coupled. Y. Zhu et al. [14] proposed another similar resonator by replacing the bottom electrode fingers with an electrode plate, as shown in Figure 5(e), achieving a k^2_{eff} up to 8% with AlN, which is comparable to the AlN-based FBAR.

Aside from the lateral modes propagating along only x or y direction of the resonator, resonators utilizing two-dimensional (2D) lateral modes were also presented and demonstrated. The 2D distributed electric field is excited by the checker-patterned electrode configuration, as shown in Figure 6. Both Lamb wave mode and LCAT mode resonators have been extended to 2D in this way, and the part with minimum displacement of the checkerboard can be further etched, to improve the k^2_{eff} to over 8% [9].

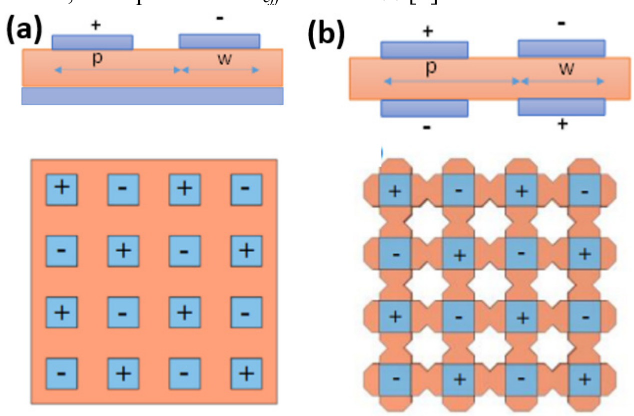

Figure 6 (a) Cross-section and top view of checker patterned Lamb wave resonator [15] (b) Cross-section and top view of checker mode LCAT mode resonator [9].

Acoustic Wave Resonators for mmWave Frequency

Traditional BAW or SAW resonators restrict frequencies to below 8GHz. However, with the burgeoning demand for mobile communications, which necessitates high network capacity, swift data transfer rates, and minimal latency, 5G technology has expanded the frequency spectrum into the mmWave range. In the high-frequency section of the 5G spectrum (from 24 GHz to 40 GHz for bands n257-n260), electromagnetic (EM) filters, such as cavity, waveguide, and microstrip filters, still dominate the market. Despite the reduction in the form factor of these EM filters in the mmWave frequency range due to lower wavelengths, their dimension remains a few millimeters, posing challenges for integrating multiple such filters into a 5G smartphone. Additionally, these filters suffer from high insertion loss and a low passband roll-off. Contrastingly, BAW/SAW filters can be miniaturized to hundreds of μm^2 area and a thickness of a few µm, making them suitable for integration in mobile devices or direct fabrication above the RF circuits for System-in-Package radio frequency front-end modules (RFFEMs). Furthermore, the low insertion loss, steep roll-off, and high out-of-band rejection of BAW/SAW filters enable adjacent band coexistence with minimal crosstalk.

While BAW/SAW filters have been successful for the sub-8GHz frequency range, advancing these technologies into the Ku-band (12 – 18 GHz) and the mmWave range presents challenges in design and fabrication, such as ultrathin piezoelectric and metal film deposition, significant impact of routing parasitics, and etching control in an ultrathin regime. The following section introduces various efforts to develop acoustic resonators and filters for the mmWave frequency range, including state-of-the-art demonstrations.

A. *XBAR resonators & filters*

To overcome the frequency limitation by the feature size of the IDT in $LiNbO_3$ (LN) and $LiTaO_3$ (LT) based SAW devices, the laterally excited bulk acoustic resonators (XBAR) based on thin film single crystal is a promising alternative to boost the frequency of LN or LT based resonators to high frequency range. To operate these devices at the millimeter-wave frequencies, the use of the higher order modes of these devices provides a possible solution.

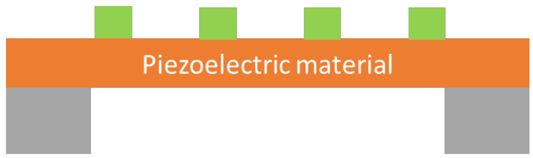

Figure 7. XBAR resonator structure

The XBAR structure can be treated as film bulk acoustic resonators with transversal excitation using IDTs as shown in Figure 7. The resonant mode of the XBAR comprises the matching composite of the two anti-symmetric Lamb modes. The resonant mode in the LN region between the two IDTs is the 1st order asymmetric (A1) mode and the 3rd order asymmetric (A3) mode in the region with the metal electrode on top of LN. The A1 and A3 modes are vertically across the LN plate, leading to the resonant frequency mainly determined by the thickness of LN. The design and performance optimization of the XBAR involves having a variation of IDT pitch, plate thickness, metal electrode thickness, and LN orientation. The IDT pitch is in several multiples of the LN plate thickness. The resonance frequency inversely scales with the plate thickness. The metal thickness has an optimum range that provides the matching between the composite A1 and A3 modes at the regions of the interface, which enables low spurious and high thermal conductance. The analytic formula for admittance Y of the XBAR resonators without the consideration of the parasitic is given by [16]:

$$Y = j\omega C_{static}\left(1 + \frac{K_t^2}{k\frac{t}{2}}\tan\left(k\,\frac{t}{2}\right)\right) \tag{1}$$

where k is the vertical wavenumber which has a dependence on the vertical shear wave velocity v and shear elastic modulus, λ is the wavelength, $\omega = 2\pi f$ is the angular frequency, and t is the thickness of the piezoelectric layer. C_{static} is the simplified static capacitance that is proportional to the number of electrodes. The K_t^2, which is the coupling coefficient of piezoelectric material, is proportional to the piezoelectric constant as per the direction of the field. The orientation of the LN should be chosen accordingly so that the piezoelectric constant values are high for the desired resonant mode.

The XBAR-based filter has been demonstrated by a company named Resonant Inc. [17]. The filter's probe measurements can provide a bandwidth of 600 MHz at 5 GHz and a bandwidth of 1200 MHz at 6 GHz. The adjacent band rejection is higher than 40 dB with a passband insertion loss of at least 2 dB.

The use of the high-order asymmetric modes with the appropriately chosen LN cut, orientation, thickness and lateral dimension enables the frequency of XBAR to be scaled towards mmWave range. However, extending to the higher-order mode limits the k^2_{eff} of the resonator inversely by the square of the order. Y. Yang et al. [18] investigated the high even order asymmetric Lamb wave modes in Z-cut LN thin film up to 60 GHz. The A3 mode at 13 GHz can achieve a k_t^2 of 3.8% while the k_t^2 of A7 mode at 30 GHz is only 0.74%. They have also demonstrated the filters based on high order Lamb wave mode resonators, achieving a 3-dB bandwidth of 70 MHz at 10.8 GHz and a fractional bandwidth of 2.93% at 14.7 GHz, respectively. [19]

Current challenges the XBAR faces involve the power handling improvement needed along with mechanical robustness, and frequency trimming [1]. To improve the power handling of XBAR, inverted XBAR [20] that comprises bottom electrodes excitation is used. The electrodes act as pedestals that provide the needed support for improving the mechanical robustness and heat dissipation directed to the substrate improves the power handling.

B. Overtone-mode Bulk Acoustic Resonator

To avoid the usage of ultrathin electrodes and piezoelectric films, bulk acoustic resonators working at high-order resonant modes, referred as overtone-mode resonators, have been presented to achieve higher frequencies. Unlike traditional FBAR or SMR working at the fundamental thickness mode, the overtone-mode resonators utilize the 2nd- or 3rd-order mode to achieve high frequency without scaling down the electrode and piezoelectric layers. However, the resonant amplitude of high-order modes is theoretically much smaller than the fundamental mode, leading to severe performance degradations in terms of low quality factor and low coupling coefficient. G. Piazza's group presented an Overmoded Bulk Acoustic Resonator (OBAR) utilizing the 2nd order overtone thickness mode to achieve a high frequency of 33.5 GHz with k^2_{eff} of 1.7% and Q of ~ 140 with 140 nm AlN sandwiched between 70 nm Pt and 90 nm Al electrode layers [21]. Unlike the traditional BAW resonators with the acoustic standing wave confined within the piezoelectric layer, the mode is split evenly between the piezoelectric and electrode layers, preventing the cancellation of symmetric polarization expansion and contraction. Besides the high-order thickness modes, the high-order Lamb-wave modes are also applied for pursuing mmWave frequency resonators. M. Assylbekova et al. presented a AlN-based Combined Overtone Resonator (COR) operating at a combined mode of the 2nd order asymmetric and the 3rd order asymmetric Lamb-wave modes (A2 & A3) [22]. This structure enables a higher resonant frequency via a thick piezoelectric film, compared to the traditional BAW resonators such as FBAR and SMR. With laterally field excitation by only top electrode, the k^2_{eff} of 0.46% and Q of ~ 254 at frequency of 23.2 GHz have been achieved.

Another type of overtone resonator is the High-Overtone Bulk Acoustic Resonators (HBAR), in which the resonator functional stack is mounted on a thick high-quality substrate, instead of air cavity or acoustic mirror to reflect the acoustic wave. Hence in an HBAR the acoustic wave can propagate into the substrate, leading to a low-frequency fundamental thickness mode at a few MHz, and a series of resonances spreading the whole frequency spectrum. Although over 40 GHz and other advantages such as controllable TCF and high quality factor have been achieved [23], the low k^2_{eff} and numerous spurious modes make it almost impossible for usage in an acoustic bandpass filter. A more realistic application of the HBAR is to evaluate the acoustic and electro-mechanical properties of thin piezoelectric films with minimum fabrication steps. C. Liu et al. [24] have taken advantage of the simplicity of HBAR structure to characterize the k_t^2 of the 100 nm and 50 nm $Sc_{0.3}Al_{0.7}N$ ultrathin films deposited by sputtering.

C. Scaling FBAR resonators and filters towards mmWave

During the last decade, continuous efforts have been denoted into scaling down the thickness and dimension of BAW resonators and filters for frequency increase with maintaining the k^2_{eff} and Q factor. M. Hara et al. [25] presented the AlN-based air-gap-type FBAR with a dome-shaped air gap beneath the resonator stack. This air gap is constructed by the deformation of the metal/piezoelectric/metal stack with a highly compressive in-plane stress. With a 120-nm AlN sandwiched between two 17-nm Ru layers, a resonator working at 24.7 GHz with k^2_{eff} of 6% and Q of ~ 280 has been demonstrated. The authors further fabricated and measured the filter composing of these air-gap-type resonators. The fractional bandwidth and the minimum insertion loss of the demonstrated filter were 3.4% and 3.8 dB, respectively. E. Iborra et al. [26] implemented an optimum AlN sputtering process with a 2-step deposition and pre-treatment to improve the thin film quality. The SMR resonators with resonant frequency of ~ 8GHz, k^2_{eff} of 6.7% and Q up to 900 have been demonstrated based on the 160 nm AlN film. M. Assylbekova et al. [27] presented Cross-sectional Lame Mode Resonators (CLMR) based on 300 nm Sc doped AlN film. With the interdigital metal electrodes, the ~ 11 GHz resonant frequency can be achieved along with lithographic tunability. C. Liu et al. [28] realized a 14.25 GHz frequency FBAR with stack of 50nm Mo/100nm $Sc_{0.2}Al_{0.8}N$/50nm Mo stack. After de-embedding the parasitics, the k^2_{eff} and quality factor of this resonator are around 8.3% and 400, respectively. With the discovery of ferroelectricity in highly Sc doped AlN in 2019, multi-layer BAW structures with alternatively poled polarization are presented to pursue high resonant frequencies. I. Merrilyn et al. [29] and D. Merrilyn et al [29] and D. Mo et al. [30] [30] independently demonstrated similar bi-piezo layer FBAR resonators reaching a resonant frequency of ~20 GHz and ~ 13.3 GHz, respectively. D. Mo's work further demonstrated the corresponding filter with an insertion loss of 2.62 dB and a fractional bandwidth of ~5.6%. Compared to traditional single piezoelectric layer structures, these alternatively poled BAW resonators enable thicker electrode layers for the same frequency, avoiding the high series parasitic resistance of the ultrathin electrode layer. Another benefit of this kind of alternative poled BAW resonator is the better power handling capacity, which is more desirable in high frequency applications. However, the intermediate electrode layer between the sub-piezoelectric layers for electrical poling raises the complexity and cost of the process. The ferroelectricity in Sc doped AlN also introduces frequency tunability in this structure, which will be further elaborated in later section.

REDUCING FOOTPRINT & FILTER NUMBER

Packaging technologies for filters, including chip scale packaging (CSP) and wafer level packaging (WLP), become critical in system integration. Post-packaged filters are interfaced with other front-end modules via on-board IO routing, which, unfortunately, introduces extra losses, parasitics, and a considerable claim on the printed circuit board (PCB) area.

Particularly in 5G systems, which may comprise up to 70 front-end filters, the combined size of packages and IO routes contributes sizably to the total PCB area. To mitigate these issues, two methods have been proposed: (i) On-chip tunable elements, permitting multiple filter responses with a single footprint. This strategy offers flexibility while reducing physical filter count, thereby conserving PCB space. (ii) Monolithic integration with CMOS IC, aiming to interface the MEMS filter directly with CMOS IC blocks, thereby eliminating inter-routing. By converging the MEMS filter and CMOS IC into a unified structure, the losses and parasitics related to routing can be reduced, enhancing performance, and further decreasing PCB footprint.

A. Ferroelectric tunable resonators and filters

On-chip tunable components can be realized by incorporating ferroelectric materials into device designs. Ferroelectricity pertains to a material's spontaneous polarization and its response to an external electric field. The direction of the polarization of a layer in a multilayer ferroelectric resonator can be adjusted to yield different resonant frequencies. Commonly used ferroelectric materials include Strontium Titanate ($SrTiO_3$), Barium Titanate ($PbZrO_3$), and the recently discovered ScAlN.

Figure 8 represents a mode-switchable resonator equipped with two ferroelectric film layers. The blue arrows demonstrate polarization direction, and the red dashed lines signify vertical displacement amplitude at resonance. If both ferroelectric layers share the same polarization, the total thickness equates to half the wavelength at the resonant frequency. If one layer's polarization is altered, the layers exhibit opposing piezoelectric orientations, vibrating in contrary directions. Consequently, the total thickness becomes twice the wavelength of the excited acoustic wave, and the resonant frequency is doubled.

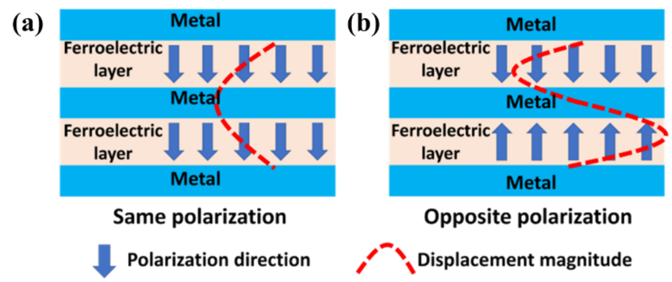

Figure 8.(a) the mode-switchable resonator with two layers of piezoelectric film, working in same polarization and (b) in opposite polarizations.

ScAlN is one of the potential candidates in tunable FBARs due to its high coupling coefficient and acoustic velocity. A bi-layer switchable FBAR using 100 nm ScAlN has been demonstrated [31], with two available resonance at 10 GHz and 18.5 GHz. D. Mo et al. from the University of Florida [32] presents a switchable resonator with two available resonances: 6.94 GHz and k^2_{eff} of 10.4% and 13.3 GHz and k^2_{eff} of 10.9%. More recently, Olsson et al. from University of Pennsylvania [33] presents an ScAlN-based resonator with resonant frequency beyond 20 GHz and coupling coefficient larger than 8% by switch the polarization of one sub-layer. In another work presented by D. Mo et al. [34], a switchable filter between 6.8 GHz and 13.3 GHz is successfully demonstrated. Besides FBAR, ScAlN applications in switchable lateral devices are presented as well [35].

The piezoelectricity in BST can be turned on and off with the presence and absence of DC field, which makes it a good material for tunable FBAR. Koohi et al. from University of Michigan [36] design a bi-layer switchable BST FBAR with one off-states (no DC voltage) and two on-states, at 1.96 GHz and 3.6 GHz. In both on-states the FBAR has a coupling coefficient exceeding 6.9%. The corresponding dual-band filter is also presented in the same work.

B. Monolithic integration

Figure 9 depicts a monolithic design of integration, vertically integrating MEMS acoustic filter with silicon-based complementary metal oxide semiconductor (CMOS) integrated circuits (IC). This arrangement dramatically reduces packaging space and parasitics, while enhancing heat dissipation. Furthermore, the process compatibility of the acoustic filter with commercial semiconductor manufacturing, with respect to thermal budget (< 350°C) and contamination issues, renders monolithic integration both viable and promising.

Literature [41] explores the feasibility of deploying MEMS devices atop CMOS processes and reports a FBAR filter, post-Low Noise Amplifier (LNA), in a 0.25µm BiCMOS process for a WCDMA front-end. The FBAR filter exhibited an insertion loss of 3dB and out-of-band rejection of 50dB. In 2019, GLOBALFOUNDRIES presented a monolithic multi-band RF front-end module (RF-FEM), integrating MEMS Lamb-wave filters and switches on a 200mm RF silicon-on-insulator (RFSOI) substrate, which reduced the footprint by up to 50% in comparison to system-in-package (SiP) modules [37]

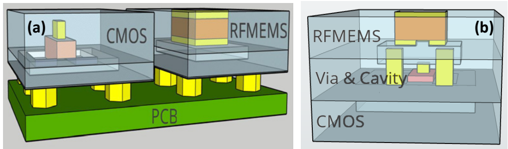

Figure 9 (a) conventional integration between CMOS circuits and MEMS device (b) monolithic integration [38]

Recently, wafer-level 3D monolithic integration of ScAlN based BAW filters with RFSOI switches is demonstrated [38]. The integrated switched filter operates at 2.5 GHz with an insertion loss of <3.6 dB and a bandwidth of >120 MHz, fitting within a compact <1 mm^2 area. The process temperature for the entire flow remains well below 400°C.

HIGH-POWER HANDLING AND MODEL OF RESONATORS AND FILTERS

Current communication system requires devices with better power handling capability to deal with larger driving power and higher frequency. At high power level, SAW/BAW filters behave nonlinearly, with a degradation in the filter response, and the generation of unwanted frequency bands, such as the second- and third-order intermodulation distortion (IMD2 and IMD3) bands. It is thus necessary to understand the mechanism and modelling method of nonlinearity in SAW/BAW filters and deduct some possible suppression methods.

A. Characterization and modelling methods of nonlinearity

The nonlinearity can be formulated by adding nonlinear terms to the piezoelectric constitutive equation:

$$T = c^E S - eE + \Delta T \qquad (2)$$
$$D = eS + \varepsilon^S E + \Delta D$$

Where T, S, D and E are the stress, strain, electric displacement, and electric field tensors, and c^E, e and ε^S are the elastic, piezoelectric, and dielectric constants. ΔT and ΔD represents the nonlinearity in the system and can be formulated as the higher order multiplications of the linear tensors [39]:

$$\Delta T_2 = \frac{1}{2}\delta_3 c^E S^2 - \delta_1 eSE + \frac{1}{2}\delta_2 \varepsilon^S E^2 \qquad (3)$$
$$\Delta D_2 = \frac{1}{2}\delta_1 eS^2 - \delta_2 \varepsilon^S SE + \frac{1}{2}\delta_4 \frac{\varepsilon^S e}{c^E} E^2$$
$$\Delta T_3 = \frac{1}{3}\gamma_4 c^E S^3 - \gamma_1 eS^2 E + \gamma_2 \varepsilon^S SE^2 + \frac{1}{3}\gamma_3 \frac{\varepsilon^S e}{c^E} E^3$$
$$\Delta D_3 = \frac{1}{3}\gamma_1 eS^3 - \gamma_2 \varepsilon^S S^2 E - \gamma_3 \frac{\varepsilon^S e}{c^E} SE^2 + \frac{1}{3}\gamma_5 \frac{(\varepsilon^S)^2}{c^E} E^3$$

A total of four second order coefficients and five third order coefficients are required to fully model the 2nd and 3rd order nonlinearity. In the case of BAW resonators where thickness extension wave dominates, all four tensors can be simplified into four 1D vectors. For resonators involving more complex acoustic waves, a detailed formulation of nonlinearity can be found in [40].

Modified Mason model employs the conventional Mason model with an extra voltage source to model the nonlinearity. Because Mason model is a 1D model, it fits well with 1D nonlinearity formulation in (3). The modified Mason model divides the piezoelectric layer into N slabs with a thickness of Δx, and the equivalent circuit of each piezoelectric sub-layer is depicted in Figure 10 (b). The values of ΔT and ΔD in two additional voltage sources can be determined by (2). By cascading the circuit of N single slabs, the overall nonlinear Mason model can be constructed and simulated using circuit simulator, such as the Keysight ADS perturbation analyzer. A nonlinear Mason model for different Sc concentration doped AlN based FBAR has been developed by [41]. By fitting the model with measured results, it shows δ_1 determines the H2 emission at resonance and δ4 determines the H2 emission off-resonance.

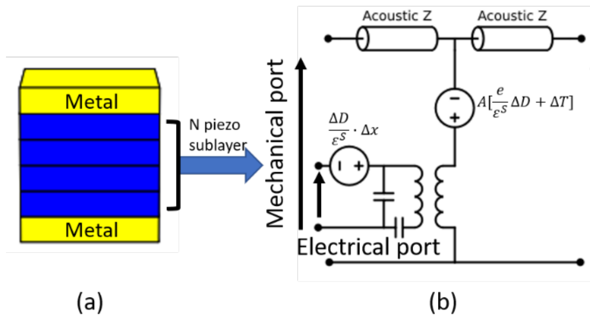

Figure 10. (a) In the 1D schematic model of FBAR, the piezoelectric film is divided into N discrete slabs, with thickness Δx. Each of these slabs is represented by a circuit, as depicted in (b), which utilized the nonlinear Mason model to characterize one sublayer of piezoelectric film. This model incorporates two current sources which represent the nonlinear terms.

The modified Mason model is constructed based on the 1D assumption. To model the nonlinearity in 3D way, finite element method (FEM) is often employed, and nonlinear terms are added to the constitutive equation as well. FEM modelling provides a more accurate representation, and however it requires analyzing the responses of multiple frequency points (H2/IMD3) under a single frequency excitation, which can be difficult in some commercial FEM software.

B. Experimental measurement of nonlinearity

Two common methods to quantify nonlinearity in RF devices, including SAW/BAW resonators, are through the harmonics measurement and the intermodulation (IMD). In harmonic measurement, a continuous wave is amplified by power amplifier (PA) to a high-power level, and then emit to the device under test (DUT), which is SAW/BAW resonator. The signal analyzer collects signals coming out from the DUT at base frequency, f_0, as well as $2f_0$ and $3f_0$, to characterize its second/ third harmonic (H2/H3) responses. The H2 and H3 responses can be used to determine the second/third-order input intercept point (IIP2/IIP3), which is the input power level when the second/third harmonic generated reaches the base frequency power level.

IMD measures the interaction of two large signals (f_1 and f_2) with a small frequency difference, at their IMD frequency $2f_1$-f_2 and $2f_2$-f_1. Figure 11 shows the schematic of IMD3 measurement. Two tones working at f_1 and f_2 are combined and transmit into the test resonator. The produced signal is then filtered by a diplexer to obtain signals at the IMD frequencies. The strength of the IMD tones indicates the level of nonlinearity in the system. Our group presents H2/IMD3 measurements on 3D monolithic integrated FBARs and filters in [38], and discovered that filters exhibit IMD3 peaks at their cutoff frequency, which are due to the series and parallel resonators.

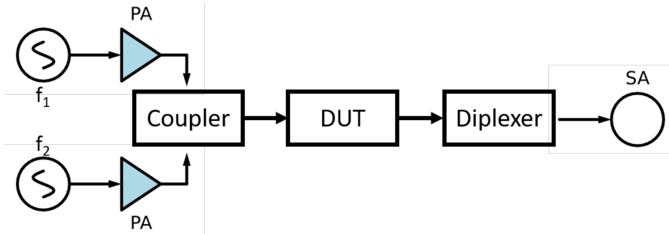

Figure 11 Block diagram for IMD3 measurement setup.

C. Suppression of nonlinearity in SAW/BAW filters

To reduce power density and suppress nonlinearity, a single resonator can be replaced by multiple resonators connected in series or parallel with opposite piezoelectric orientation. Handtmann et al. [42] presents how this method helps to reduce the H2 response of a filter by about 20 dB. Feld et al. [43] describes the trade-offs with parallel connected and series connected FBARs, which are referred to as split-BAR (parallel connected) and power-BAR (series connected), shown in Figure 12. Both structures can provide a larger linear input power range than a single resonator, while the split-BAR shows degradation in quality factor due to a larger perimeter to area ratio, and the power-BAR has a larger footprint. The application of split-BAR and power-BAR requires delicate area optimization. Ivira et al. [44] presents a 6-FBARs split-3BAR structure, which shows a good balance between nonlinearity reduction and device footprint. By optimizing the area and shape of each FBAR, the final design has comparable H2 and IMD3 responses to the well-known quad-BAR structure (four series connected FBAR with 16x active area), and better power handling capability, with only 9x active area.

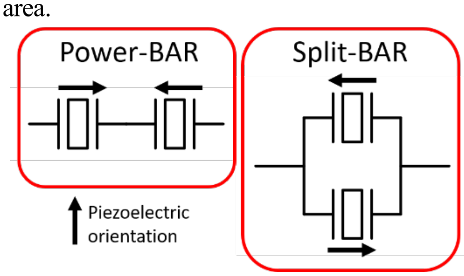

Figure 12 Block diagram of power-BAR and split-BAR, the black arrow indicates the piezoelectric orientation.

In terms of SAW resonator, similar methodology of trading nonlinearity with device area are employed. By enlarging the IDT area, the heat density can be reduced to avoid nonlinearity occurrence. Other than that, using multilayer substrate of more linear material is another way to reduce nonlinearity in both SAW and BAW resonators.

Conclusions

With the rapid progression in the domain of microwave acoustic wave devices, significant optimism surrounds the future of RF filters. SAW and BAW technologies are leading the innovation front, showing considerable promise. As we advance towards 5G networks and beyond, the influence of these microwave acoustic wave devices on wireless communication technologies is profound. With increasing demand for higher data rates, reduced latency, and superior connectivity, RF filters are subjected to escalated performance, size, and cost demands. Innovations within SAW and BAW technologies have risen to these challenges, pushing the boundaries of traditional expectations. The continuous evolution is palpable, with the introduction of new materials like Sc-doped AlN and innovative structures such as IHP SAW and XBAR playing a significant role in advancing the field. Furthermore, developments in monolithic integration are setting a new benchmark, enhancing the potential of acoustic resonator technology substantially. New material and fabrication techniques are enabling the creation of RF filters with heightened frequency capacity and robustness under strenuous conditions, thus expanding application possibilities.

In conclusion, the persistent advancements in microwave acoustic wave devices promise a bright future for RF filters. Their pivotal role in accommodating the burgeoning demands of wireless communication technologies, from current 5G networks to prospective future wireless systems, is increasingly apparent.

Acknowledgment

This work was supported by the Science and Engineering Research Council of A*STAR (Agency for Science, Technology, and Research) Singapore, under Grant No. A20G9b0135.

References

[1] A. Hagelauer, R. Ruby, S. Inoue, V. Plessky, K.-Y. Hashimoto, R. Nakagawa, J. Verdu, P. d. Paco, A. Mortazawi, G. Piazza, Z. Schaffer, E. T.-T. Yen, T. Forster and A. Tag, "From Microwave Acoustic Filters to Millimeter-Wave Operation and New Applications," *IEEE Journal of Microwaves,* vol. 3, no. 1, pp. 484-508, 1 2023.

[2] C. C. W. Ruppel, "Acoustic Wave Filter Technology–A Review," *IEEE Transactions on Ultrasonics, Ferroelectrics, and Frequency Control,* vol. 64, no. 9, pp. 1390-1400, 9 2017.

[3] T. Takai, H. Iwamoto, Y. Takamine, H. Yamazaki, T. Fuyutsume, H. Kyoya, T. Nakao, H. Kando, M. Hiramoto, T. Toi, M. Koshino and N. Nakajima, "Incredible high performance SAW resonator on novel multi-layerd substrate," *2016 IEEE International Ultrasonics Symposium (IUS),* pp. 1-4, 9 2016.

[4] T. Takai, H. Iwamoto, Y. Takamine, T. Nakao, M. Hiramoto and M. Koshino, "I.H.P. SAW technology and its application to micro acoustic components," *2017 IEEE International Ultrasonics Symposium (IUS),* pp. 1-1, 9 2017.

[5] T. Takai, H. Iwamoto, Y. Takamine, T. Fuyutsume, T. Nakao, M. Hiramoto, T. Toi and M. Koshino, "High-Performance SAW Resonator With Simplified LiTaO3 SiO 2 Double Layer Structure on Si Substrate," *IEEE Transactions on Ultrasonics, Ferroelectrics, and Frequency Control,* vol. 66, no. 5, pp. 1006-1013, 5

2019.

[6] L. Chen, C. Liu, M. Li, W. Song, W. Wang, Z. Wang, N. Wang and Y. Zhu, "Scandium-Doped Aluminum Nitride for Acoustic Wave Resonators, Filters, and Ferroelectric Memory Applications," 2023.

[7] J. Zhou, Y. Liu, Q. Xu, Y. Xie, Y. Cai, J. Liu, W. Liu, A. Tovstopyat and C. Sun, "ScAlN/AlN Film-Based Lamé Mode Resonator With High Effective Electromechanical Coupling Coefficient," *Journal of Microelectromechanical Systems,* vol. 30, no. 5, pp. 677-679, 10 2021.

[8] Z. Luo, S. Shao, K. Liu, Y. Lu, A. Mazzalai, C. Tosi and T. Wu, "Al0.7Sc0.3N butterfly-shaped laterally vibrating resonator with a figure-of-merit (k t2·Q m) over 146," *Applied Physics Letters,* vol. 120, no. 17, p. 173508, 4 2022.

[9] Y. Zhu, N. Wang, C. Sun and Y. Zhang, "Design of AlN Meshed LCAT Mode Resonators for Coupling Coefficient Beyond BAW," *2019 IEEE International Ultrasonics Symposium (IUS),* pp. 1717-1719, 10 2019.

[10] C. Cassella, Y. Hui, Z. Qian, G. Hummel and M. Rinaldi, "Aluminum Nitride Cross-Sectional Lamé Mode Resonators," *Journal of Microelectromechanical Systems,* vol. 25, no. 2, pp. 275-285, 4 2016.

[11] Y. Zhu, N. Wang, G. Chua, C. Sun, N. Singh and Y. Gu, "ScAlN-Based LCAT Mode Resonators Above 2 GHz With High FOM and Reduced Fabrication Complexity," *IEEE Electron Device Letters,* vol. 38, no. 10, pp. 1481 - 1484, 2017.

[12] C. Cassella and G. Piazza, "AlN Two-Dimensional-Mode Resonators for Ultra-High Frequency Applications," *IEEE Electron Device Letters,* vol. 36, no. 11, pp. 1192-1194, 11 2015.

[13] C. Liu, Y. Zhu, B. Chen and N. Wang, "SC0.15Al0.85N-based 4 GHz Coupled Bulk Acoustic Resonators (CBAR) and Filters for the Single-Chip Duplexer Solution," in *2021 IEEE International Ultrasonics Symposium (IUS)*, Xi'an, 2021.

[14] Y. Zhu, N. Wang, B. Chen and Y. Zhang, "AlN BAW-like Resonators with Patterned Top Electrodes Achieving Coupling Coefficient up to 8% at 2.5GHz," *2019 IEEE International Ultrasonics Symposium (IUS),* pp. 93-95, 10 2019.

[15] Y. Zhu, N. Wang, G. L. Chua, B. Chen, M. Srinivas, N. Singh and Y. Gu, "Quality Factor Improvement of a 2.4GHz AlN Checker Patterned Lamb Wave Resonator by Novel Distributed Anchor Design," *2018 IEEE International Ultrasonics Symposium (IUS),* pp. 1-4, 10 2018.

[16] S. Yandrapalli, S. E. K. Eroglu, V. Plessky, H. B. Atakan and L. G. Villanueva, "Study of Thin Film LiNbO3 Laterally Excited Bulk Acoustic Resonators," *Journal of Microelectromechanical Systems,* vol. 31, no. 2, pp. 217-225, 4 2022.

[17] J. Koulakis, J. Koskela, W. Yang, L. Myers, G. Dyer and B. Garcia, "XBAR physics and next generation filter design," *2021 IEEE International Ultrasonics Symposium (IUS),* pp. 1-5, 9 2021.

[18] Y. Yang, R. Lu, L. Gao and S. Gong, "10–60-GHz Electromechanical Resonators Using Thin-Film Lithium Niobate," *IEEE Transactions on Microwave Theory and Techniques,* vol. 68, no. 12, pp. 5211-5220, 12 2020.

[19] L. Gao, Y. Yang and S. Gong, "A 14.7 GHz Lithium Niobate Acoustic Filter with Fractional Bandwidth of 2.93%," in *IEEE International Ultrasonics Symposium (IUS)*, 2020.

[20] V. Plessky, "XBAR," *2022 IEEE International Ultrasonics Symposium (IUS),* pp. 1-11, 10 2022.

[21] Z. Schaffer, P. Simeoni and G. Piazza, "33 GHz Overmoded Bulk Acoustic Resonator," *IEEE Microwave and Wireless Components Letters,* vol. 32, no. 6, pp. 656-659, 6 2022.

[22] M. Assylbekova, G. Chen, M. Pirro, G. Michetti and M. Rinaldi, "Aluminum Nitride Combined Overtone Resonator for Millimeter Wave 5g Applications," in *2021 IEEE 34th International Conference on Micro Electro Mechanical Systems (MEMS)*, 2021.

[23] B. P. Sorokin, N. O. Asafiev, G. M. Kvashnin, D. A. Scherbakov, S. A. Terentiev and V. D. Blank, "Toward 40 GHz excitation of diamond-based HBAR," *Applied Physics Letters,* vol. 118, no. 8, 2 2021.

[24] C. Liu, M. Li, N. Wang and Y. Zhu, "Sub-100nm Al0.7Sc0.3N Thin Films for Next Generation Bulk Acoustic Wave Resonators and Filters," *2022 IEEE International Ultrasonics Symposium (IUS),* pp. 1-3, 10 2022.

[25] M. Hara, T. Yokoyama, T. Sakashita, S. Taniguchi, M. Iwaki, T. Nishihara, M. Ueda and Y. Satoh, "Super-High-Frequency Band Filters Configured with Air-Gap-Type Thin-Film Bulk Acoustic Resonators," *Japanese Journal of Applied Physics,* vol. 49, no. 7S, p. 07HD13, 7 2010.

[26] E. Iborra, M. Clement, J. Capilla, J. Olivares and V. Felmetsger, "Optimization of thin AlN sputtered films for X-band BAW resonators," *2010 IEEE International Ultrasonics Symposium,* pp. 1688-1691, 10 2010.

[27] M. Assylbekova, M. Pirro, X. Zhao, G. Michetti, P. Simeoni and M. Rinaldi, "Study of the Performance Enhancement of Sc-Doped AlN Super High Frequency Cross-Sectional Lamé Mode Resonators," *Micromachines,* vol. 14, no. 3, p. 515, 2 2023.

[28] C. Liu, X. Wang, W. Yang, Y. Zhang, E. Y. Woo and Y. Zhu, "A Sc0.2Al0.8N-based 14GHz Film Bulk Acoustic Resonator with over 8% Coupling Coefficient and over 400 Quality factor for Ku-band applications," *IEEE IEEE International Ultrasonics Symposium (IUS) 2023.*

[29] Izhar, M. M. A. Fiagbenu, P. Musavigharavi, X. Du, J.

Leathersich, C. Moe, A. Kochhar, E. A. Stach, R. Vetury and R. H. Olsson, "A K-Band Bulk Acoustic Wave Resonator Using Periodically Poled Al0.72 Sc0.28N," 2023.

[30] D. Mo, S. Dabas, S. Rassay and R. Tabrizian, "A C/K u Dual-Band Reconfigurable Baw Filter Using Polarization Tuning in Layered Scaln," *2023 IEEE 36th International Conference on Micro Electro Mechanical Systems (MEMS),* pp. 1179-1182, 1 2023.

[31] C. Li, "Impact of Asymmetric Piezoelectricity of 100 nm Al0.7Sc0.3N Thin Film on Ferroelectrically Switchable Multi-Layer Bulk Acoustic Wave Resonators," *Proceedings, 2023 Joint Conference of the IEEE International Frequency Control Symposium and the European Frequency and Time Forum, Toyama, Japan, to be published.,* 2023.

[32] D. Mo, S. Dabas, S. Rassay and R. Tabrizian, "Complementary-Switchable Dual-Mode SHF Scandium Aluminum Nitride BAW Resonator," *IEEE Transactions on Electron Devices,* vol. 69, no. 8, pp. 4624-4631, 8 2022.

[33] Izhar, M. M. A. Fiagbenu, P. Musavigharavi, X. Du, J. Leathersich, C. Moe, A. Kochhar, E. A. Stach, R. Vetury and R. H. Olsson, "A K-Band Bulk Acoustic Wave Resonator Using Periodically Poled Al0.72Sc0.28N," *IEEE Electron Device Letters,* vol. 44, no. 7, pp. 1196-1199, 7 2023.

[34] D. Mo, S. Dabas, S. Rassay and R. Tabrizian, "A C/Ku Dual-Band Reconfigurable Baw Filter Using Polarization Tuning in Layered ScalN," *2023 IEEE 36th International Conference on Micro Electro Mechanical Systems (MEMS),* pp. 1179-1182, 1 2023.

[35] V. Gund, K. Nomoto, H. G. Xing, D. Jena and A. Lal, "Intrinsically Switchable GHz Ferroelectric ScAlN SAW Resonators," *2022 IEEE International Symposium on Applications of Ferroelectrics (ISAF),* pp. 1-4, 6 2022.

[36] M. Z. Koohi and A. Mortazawi, "Negative Piezoelectric-Based Electric-Field-Actuated Mode-Switchable Multilayer Ferroelectric FBARs for Selective Control of Harmonic Resonances Without Degrading Keff^2," *IEEE Transactions on Ultrasonics, Ferroelectrics, and Frequency Control,* vol. 67, no. 9, pp. 1922-1930, 9 2020.

[37] H. Campanella, Y. Qian, C. Romero, J. J. Giner and R. Kumar, "Integrated Filter and RF Front-end Module on RF SOI," *2019 Electron Devices Technology and Manufacturing Conference (EDTM),* pp. 395-397, 3 2019.

[38] Y. Zhang, X. Wang, C. Liu, E. Y. Z. Woo, W. Yang, Q. Zhang, H. Lin, D. Yan, R. M. Kumarasamy, B. Chen, N. Wang and Y. Zhu, "3D Monolithic Integration of ScAlN-based GHz MEMS Acoustic Filters on 200mm RFSOI Wafer," *2022 International Electron Devices Meeting (IEDM),* pp. 16.2.1-16.2.4, 12 2022.

[39] D. A. Feld, D. S. Shim, S. Fouladi and F. Bayatpur, "Advances in nonlinear measurement & modeling of bulk acoustic wave resonators (invited)," *2014 IEEE International Ultrasonics Symposium,* pp. 264-272, 9 2014.

[40] A. Mayer, "Surface acoustic waves in nonlinear elastic media," *Physics Reports,* vol. 256, no. 4-5, pp. 237-366, 5 1995.

[41] Y. Zhang, W. Yang, C. Liu, X. Wang, E. W. Yi Zhun, N. Wang and Y. Zhu, "Experimental and Numerical Study on the Second Order Harmonic (H2) and Third Order Intermodulation Distortion (IMD3) Response of Scandium Aluminum Nitride Based FBAR Devices with Different Scandium Doping Levels," *2022 IEEE International Ultrasonics Symposium (IUS),* pp. 1-3, 10 2022.

[42] M. Handtmann, B. Gebauer, M. Franosch and K. Mutamba, "Stacked crystal resonator: A highly linear BAW device," *2009 IEEE International Ultrasonics Symposium,* pp. 889-892, 9 2009.

[43] D. A. Feld, S. Fouladi, P. Bradley, J. Larson and R. Ruby, "Unbalanced device comprised of FBAR resonators," *2012 IEEE International Ultrasonics Symposium,* pp. 71-76, 10 2012.

[44] B. Ivira, J. Larson, I. Ruby, T. Jamneala, C. Kirkendall, D. Figueredo, L. Kekoa and R. Ruby, "Integrated split 3-BAR resonator structure for higher power handling capability," *2016 IEEE International Ultrasonics Symposium (IUS),* pp. 1-6, 9 2016.